

# *Superparamagnetic Ni:SiO<sub>2</sub>–C nanocomposites films synthesized by a polymeric precursor method*

**Journal of Nanoparticle Research**  
An Interdisciplinary Forum  
for Nanoscale Science and  
Technology

ISSN 1388-0764  
Volume 13  
Number 2

J Nanopart Res (2010)  
13:703-710  
DOI 10.1007/  
s11051-010-0068-2



**Your article is protected by copyright and all rights are held exclusively by Springer Science+Business Media B.V.. This e-offprint is for personal use only and shall not be self-archived in electronic repositories. If you wish to self-archive your work, please use the accepted author's version for posting to your own website or your institution's repository. You may further deposit the accepted author's version on a funder's repository at a funder's request, provided it is not made publicly available until 12 months after publication.**

# Superparamagnetic Ni:SiO<sub>2</sub>–C nanocomposites films synthesized by a polymeric precursor method

F. C. Fonseca · R. F. Jardim · M. T. Escote ·  
 P. S. Gouveia · E. R. Leite · E. Longo

Received: 20 April 2010/Accepted: 16 August 2010/Published online: 2 September 2010  
 © Springer Science+Business Media B.V. 2010

**Abstract** In this work, we report on the magnetic properties of nickel nanoparticles (NP) in a SiO<sub>2</sub>–C thin film matrix, prepared by a polymeric precursor method, with Ni content  $x$  in the 0–10 wt% range. Microstructural analyses of the films showed that the Ni NP are homogeneously distributed in the SiO<sub>2</sub>–C matrix and have spherical shape with average diameter of  $\sim 10$  nm. The magnetic properties reveal features of superparamagnetism with blocking temperatures  $T_B \sim 10$  K. The average diameter of the Ni NP, estimated from magnetization measurements, was found to be  $\sim 4$  nm for the  $x = 3$  wt% Ni sample, in excellent agreement with X-ray diffraction data.

M versus H hysteresis loops indicated that the Ni NP are free from a surrounding oxide layer. We have also observed that coercivity ( $H_C$ ) develops appreciably below  $T_B$ , and follows the  $H_C \propto [1 - (T/T_B)^{0.5}]$  relationship, a feature expected for randomly oriented and non-interacting nanoparticles. The extrapolation of  $H_C$  to 0 K indicates that coercivity decreases with increasing  $x$ , suggesting that dipolar interactions may be relevant in films with  $x > 3$  wt% Ni.

**Keywords** Polymeric precursor method · Spin coating · Nickel nanoparticles · Superparamagnetism

## Introduction

Recently, the magnetic properties of nanoparticles have been the focus of intense scientific activities. These activities are directly related to large commercialization perspectives of potential application of magnetic systems in ultrahigh-density data storage and drug delivery. Such applications involve the miniaturization of the components and rely on magnetic properties that are stable with time. However, the size reduction of devices is limited by the fundamental magnetic properties of the ferromagnetic materials. When the size of magnetic particles is reduced to dimensions in which the magnetic anisotropy energy is comparable to the thermal energy, the magnetic moments are induced to flip randomly with time. In this state, the magnetic particles lose their

F. C. Fonseca (✉)  
 Instituto de Pesquisas Energéticas e Nucleares,  
 São Paulo, SP 05508-000, Brazil  
 e-mail: fcfonseca@ipen.br

R. F. Jardim  
 Instituto de Física, Universidade de São Paulo,  
 CP 66318, São Paulo, SP 05315-970, Brazil

M. T. Escote  
 Universidade Federal do ABC, Santo André,  
 SP 09210-170, Brazil

P. S. Gouveia · E. R. Leite  
 LIEC, Universidade Federal de São Carlos,  
 CP 676, São Carlos, SP 13565-905, Brazil

E. Longo  
 Instituto de Química, Universidade Estadual Paulista,  
 Araraquara, SP 14800-900, Brazil

ordering and become superparamagnetic (Skumryev et al. 2003).

One of the main issues concerning ferromagnetic nanoparticles is the assembling of systems for use in practical devices. In order to avoid the agglomeration and to allow an easier handling of high surface area particles, different approaches have been demonstrated, including ferrofluids and particles embedded in a non-magnetic matrix, either as powder or as thin films. Thin films of ferromagnetic particles in an amorphous SiO<sub>2</sub> matrix have been produced by several different techniques aiming for possible technological applications (Munford et al. 2001). Several techniques, such as sputtering (Tomita et al. 2004; Zhu et al. 2009; Fonseca et al. 2005), laser ablation (Dureuil et al. 2001), electrodeposition (Osaka 2000), nanolithography (Liu et al. 2004; Hong and Mirkin 2000), and by wet chemistry routes (Almeida et al. 2003; Kockrick et al. 2007) have been reported for the fabrication of superparamagnetic nanocomposites. However, it has been found that the magnetic properties of systems in the nanometric scale are strongly dependent on the preparation technique, which can result in particles with different size distributions and morphology, and possible interactions with the matrix.

In addition, metallic nanoparticles are highly reactive and tend to be oxidized, usually forming a core–shell structure comprised of a metallic core and an oxide layer over the surface of the particles. The core–shell structure can result in different magnetic properties due to the coupling of the ferromagnetic core to the antiferromagnetic oxide layer, known as exchange bias (Sharma et al. 2010).

Within this context, this study aims at the production of superparamagnetic films of Ni nanoparticles embedded in an amorphous SiO<sub>2</sub>–C matrix. Thin films were prepared by the deposition of a polymeric precursor resin by spin coating with different concentrations of the metallic phase. Detailed microstructural and magnetic characterizations revealed that the samples exhibit superparamagnetic behavior and absence of an oxide layer surrounding the Ni NP. In addition, parameters extracted from a model of non-interacting superparamagnetic particles were found to be in good agreement with the microstructural properties for the most diluted samples, in which dipolar interactions are more likely to be absent.

## Experimental

The polymeric precursor synthesis was used for producing Ni nanoparticles (NP) embedded into an amorphous silica matrix (*x*-Ni:SiO<sub>2</sub>–C). All reagents used were pro analysis grade with purity >99%. The precursor resin was synthesized by the dissolution of citric acid (Merck) in 20 mL of ethanol. After a clear solution was obtained, tetraethylorthosilicate (TEOS, Aldrich) was added, followed by hexahydrated nickel nitrate (Merck), previously dissolved in 10 mL of ethanol. The metallic citrate was kept under magnetic stirring for ~120 min. Then, ethylene glycol (Aldrich) was added to promote the polymerization of the metallic citrate. Following this procedure, samples with different Ni concentrations (*x*), in the 0–10 wt% range, have been prepared by controlling the stoichiometric ratio between Ni nitrate and TEOS.

The viscosity of precursor resins with different Ni content was adjusted between 4.0 and 5.5 mPa s previous to the spin coat deposition (Zanetti et al. 1999). Silicon (100) substrates were used with a spin-coater (Chematec Technology, KW-4B) with rotation speed set to 5,000 rpm for 20 s (Rangel et al. 2002). After the deposition of each layer, a drying step at 45 °C in a hot plate was carried out for elimination of solvent excess. The organic matter of deposited films was then partially removed by heat treatments in flowing N<sub>2</sub> at 250 °C for 100 min and 550 °C for 120 min. The total reduction to Ni is assured by an additional heat treatment at 500°C for 60 min under H<sub>2</sub> flow.

The Ni content of the films was determined by flame absorption atomic spectroscopy (FAAS) using a Varian AA-800 equipment. The produced films *x*-Ni:SiO<sub>2</sub>–C, with nominal compositions *x* = 0, 5, and 10 wt%, were characterized by X-ray diffraction by using a Rigaku D/Max 2500 PC diffractometer with Cu K<sub>α</sub> radiation, in the  $5 \leq 2\theta \leq 75^\circ$  range, with step size of 0.02°, and counting time of 4 s. Microstructural analyses of the thin films were carried out by using an atomic force microscopy (AFM) Digital Instruments Nanoscope III-A, a high-resolution scanning electron microscopy (HR-SEM) Zeiss Supra 35, and a transmission electron microscopy (TEM) Philips 200 kV. HR-SEM images were performed on uncoated films surfaces. For TEM analysis, the films were detached from the substrate and broken using a pulsed ultrasonic probe in water and deposited on a carbon-covered copper grid.

The magnetic characterization of the thin films was performed in a Quantum Design SQUID magnetometer under applied magnetic fields ( $H$ ) ranging between  $-7$  and  $7$  T and in the temperature ( $T$ ) window  $2$ – $300$  K. The temperature dependence of magnetization  $M(T)$  was measured in both zero-field-cooling (ZFC) and field-cooling (FC) modes at several applied magnetic fields.

## Results and discussions

The Ni content of the  $x$ -Ni:SiO<sub>2</sub>–C films has been evaluated by atomic absorption spectroscopy (FAAS) and the results, displayed in the Table 1, show that the estimated values,  $x = 3$  and  $6$  wt% Ni, are slightly lower than their respective nominal ones ( $x = 5$  and  $10$  wt%). Such a discrepancy may be related to: (i) some preferential evaporation during the production of the thin films; and/or (ii) to the presence of residual amorphous carbon after the heat treatments.

The X-ray diffraction analysis revealed the crystalline phases of the thin films (Gouveia et al. 2005; Carreño et al. 2002; Lee and Kim 2001). Figure 1a shows the XRD pattern of the  $x = 6$  wt% Ni sample in the  $2\theta$  region of the maximum relative intensity peak associated to Ni at  $2\theta \sim 44.45^\circ$ , which corresponds to the 111 plane of the fcc structure (Fm3m) with estimated lattice parameter of  $\sim 0.3495$  (0,0018) nm. In addition to broad peaks belonging to Ni, XRD patterns in the entire  $2\theta$  range (not shown) exhibit peaks associated with the Si substrate (at  $2\theta \sim 33^\circ$ ,  $62^\circ$ , and  $69^\circ$ ), and a halo indexed at  $2\theta \sim 22^\circ$  as belonging to the amorphous SiO<sub>2</sub>–C matrix (Gouveia et al. 2005). By using the XRD data and the Scherrer equation, the average crystallite size  $D_{XRD}$  of Ni in the thin films were estimated to be

$\sim 3.2$  and  $5.6$  nm for samples Ni:SiO<sub>2</sub>–C with  $3$  and  $6$  wt% Ni, respectively.

Figure 1b shows an AFM image of the  $x = 3$  wt% Ni sample, in which it is possible to observe a granular structure of nearly spherical clusters with average size of  $\sim 50$  nm and a relatively uniform topography. Previously reported atomic force analysis allowed for the estimation of the surface roughness  $R = 24$  and  $8.2$  nm for the films with  $0$  and  $6$  wt% Ni, respectively (Gouveia et al. 2005). Cross section images shown in Fig. 1c revealed that the thickness of the film with no metal addition was  $\sim 550$  nm, while films with Ni particles were close to  $1000$  nm, a difference certainly related to different viscosities of the precursor resins.

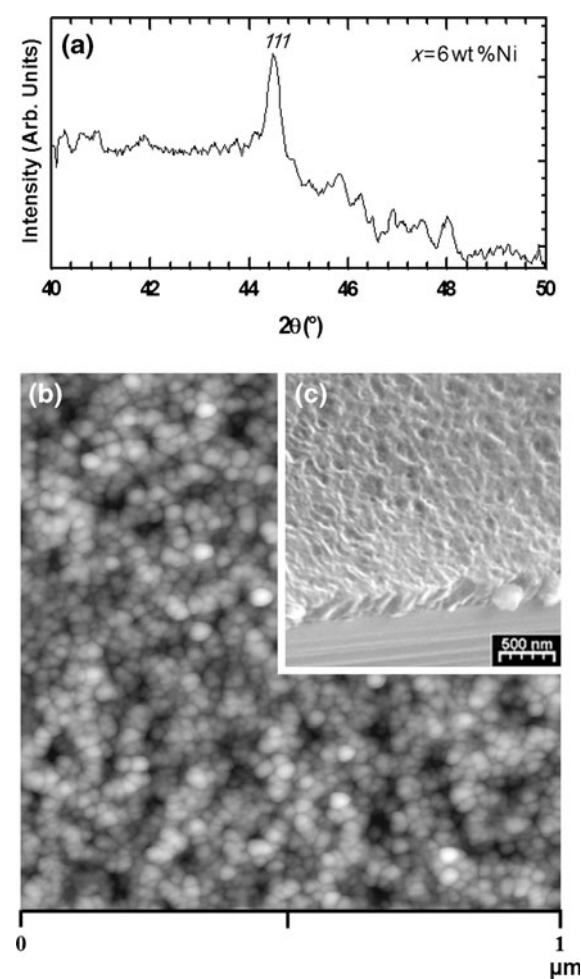


**Table 1** Values of the Ni content of the  $x$ -Ni:SiO<sub>2</sub>–C thin films (in wt%), average particle sizes determined from scanning electron microscopy ( $D_{HR-SEM}$ ), crystallite size ( $D_{XRD}$ ), and average size estimated from magnetization data ( $D_{TB}$ )

%Ni	$D_{HR-SEM}$ (nm)	$D_{XRD}$ (nm)	$D_{TB}$ (nm)
3	7	3.2	3.9
6	9	5.6	4.6

**Fig. 1** X-ray diffraction pattern of the sample with  $x = 6$  wt% Ni (a), atomic force image of sample with  $x = 3$  wt% Ni (b), and cross section scanning electron microscopy image of the film without Ni (c)

The microstructural properties of the films were further investigated by both scanning (HR-SEM) and transmission (TEM) electron microscopies, as displayed in Fig. 2. The HR-SEM analysis (Fig. 2a) revealed that the Ni:SiO<sub>2</sub>–C films have a uniform surface topography and a low porosity. In addition, both HR-SEM and TEM analyses indicated that the films have a homogeneous distribution of spherically shaped Ni nanoparticles in the ceramic matrix, as inferred from the images of Fig. 2a and b. The HR-SEM images were also used to construct the Ni particle size log-normal distribution for both  $x = 3$  and 6 wt% Ni samples. The obtained distributions are

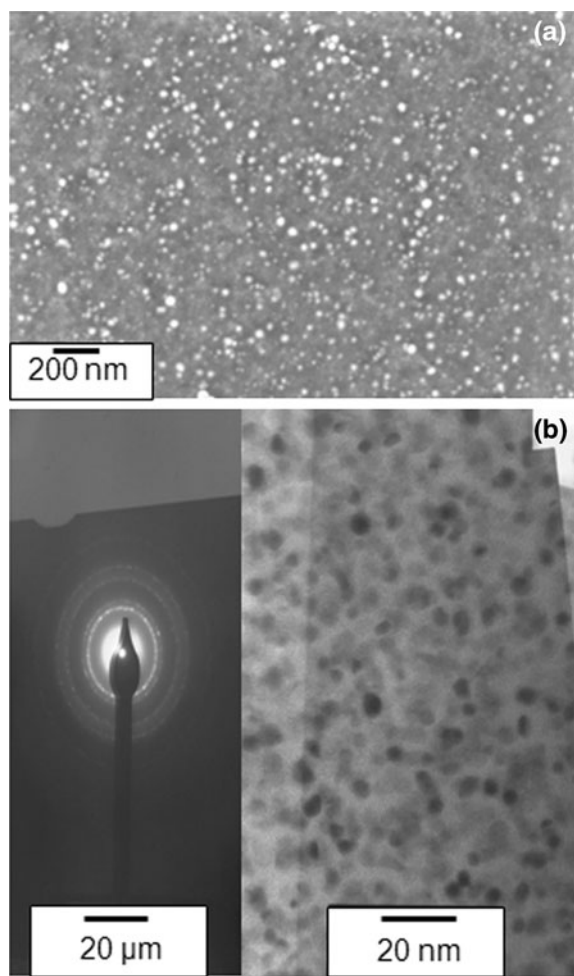


**Fig. 2** Scanning electron microscopy (**a**) and transmission electron microscopy with electron diffraction pattern (**b**) of the samples: **a**  $x = 6$  wt% Ni and **b**  $x = 3$  wt% Ni. The Ni nanoparticles correspond to brighter spots in **a** and to the darker ones in **b**

displayed in Fig. 3, and the average particle sizes are summarized in Table 1. Increasing Ni concentration results in a broader size distribution and an increase of the average particle sizes ( $\sim 7$  and  $\sim 9$  nm for  $x = 3$  and 6 wt% Ni, respectively), indicating the coalescence of metallic particles. These values are greater than the ones obtained from the Scherrer equation using XRD data. However, it is important to consider that size distributions derived from HR-SEM images are actually less accurate due to the relatively low resolution ( $\sim 3.5$  nm) of the technique, which favors the counting of larger particles. The particle size can be better assessed from the TEM image. A visual inspection of Fig. 2c indicates that a considerable fraction of Ni particles have sizes below 10 nm. In addition to this, electron diffraction data, displayed in

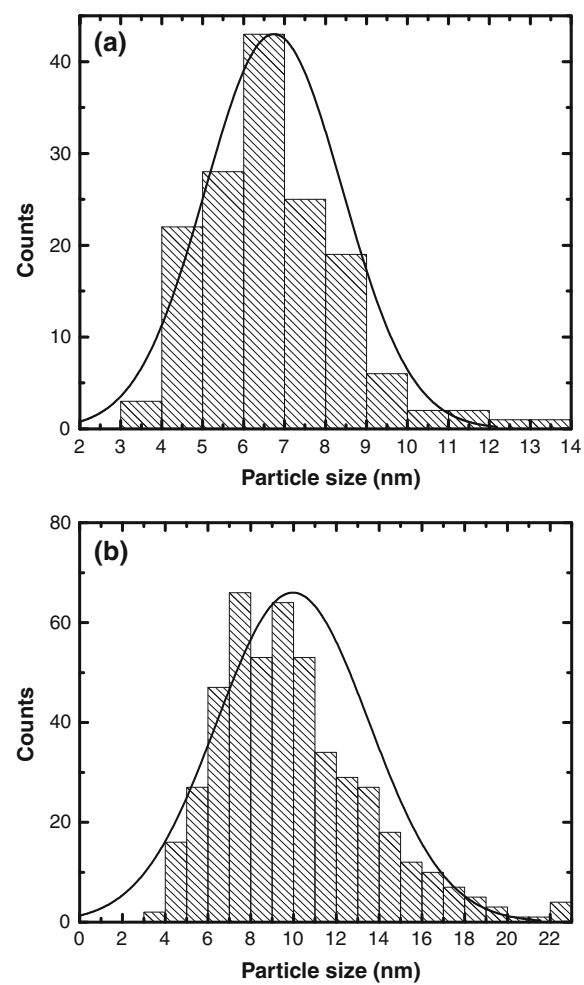


**Fig. 3** Particle size distributions of samples **a**  $x = 3$  wt% Ni and **b**  $x = 6$  wt% Ni

Fig. 2b, confirmed the cubic structure of metallic fcc Ni. In fact, the analysis of Fig. 2 indicate spots corresponding to the (400) diffraction peak, further suggesting the formation of cubic metallic Ni, in good agreement with the XRD results.

The magnetic properties of the thin films were inferred from measurements of magnetization as a function of both temperature and applied magnetic fields  $M(H,T)$ . The superparamagnetic behavior observed in the  $x$ -Ni:SiO<sub>2</sub>–C thin films was thus correlated to their microstructural properties. We first consider the temperature dependence of the magnetization and magnetic susceptibility  $\chi(T)$ , as displayed in Fig. 4a and b, respectively. The Fig. 4a displays the temperature dependence of the magnetization  $M(T)$  under an applied magnetic field  $H = 500$  Oe and the inset an expand view for temperatures below  $\sim 50$  K, for films with 3 and 6 wt% Ni. The nanometric size of the Ni particles leads to a magnetic monodomain behavior below the blocking temperature  $T_B$ . Above  $T_B$ , both the systems exhibit superparamagnetism, i.e., the magnetic susceptibility decreases monotonically with increasing temperature and assumes values well above the ones usually observed in paramagnetic materials. The measured curves display typical features of superparamagnetic systems (SPM): (i) a rounded maximum on the ZFC curve occurring at  $T_B \sim 10$  K, which is associated with the blocking of the nanoparticles; and (ii) for temperatures above  $T_B$ , the  $M(T)$  increases with decreasing  $T$ . The estimated values of  $T_B$  are  $\sim 7$  and 11 K for samples with 3 and 6 wt% Ni, respectively. Previous  $M(H, T)$  measurements on  $x$ -Ni:SiO<sub>2</sub>–C powder nanocomposites, prepared by similar procedure, revealed superparamagnetic behavior above  $T_B \sim 20$  K, but the average size of the Ni NP was bigger (Fonseca et al. 2003). In that study, the average particle size was estimated by using the  $M(H, T)$  data to be  $\sim 7$  nm, a value confirmed by both XRD and TEM analyses (Fonseca et al. 2002, 2003). The  $T_B$  value is associated with the particle size distribution and the higher is the particle size the higher is  $i_B$ . In this study,  $T_B$  values are considerably lower, suggesting that the metal particle size in the  $x$ -Ni:SiO<sub>2</sub>–C thin films is smaller than in powder nanocomposites.

The blocking temperature of a randomly oriented and non-interacting system of nanoparticles can be estimated by using the relationship

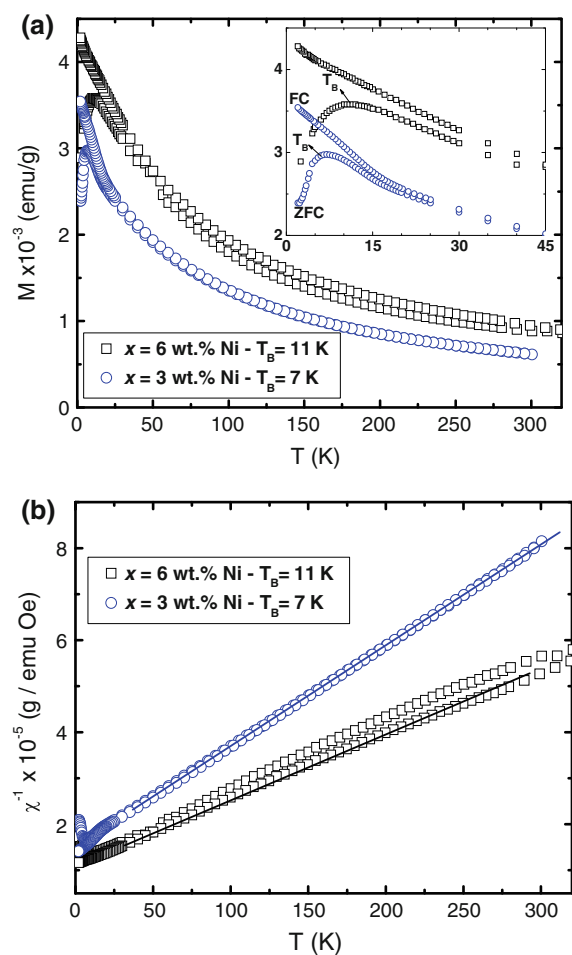


**Fig. 4** Temperature dependence of the magnetization (a) and DC magnetic susceptibility (b) for the thin films Ni:SiO<sub>2</sub>–C with  $x = 3$  and 6 wt% Ni. The *inset* in a displays an expanded view of the temperature dependence of the magnetization for  $T < 50$  K. The ZFC and FC branches and the blocking temperature  $T_B$  are also indicated

$$T_B = K\langle V \rangle / 25 k_B \quad (1)$$

where  $K = 8 \times 10^5$  ergs/cm<sup>3</sup> (Bozorth 1956) is the magnetic anisotropy constant of Ni,  $\langle V \rangle$  is the average volume of particles and  $k_B$  the Boltzmann constant (Stoner and Wohlfarth 1948). By using the measured  $T_B$  values for the Ni thin films, the diameter of assumed spherical particles have been estimated and are listed in the Table 1. The calculated values are in excellent agreement with the crystallite size evaluated from the XRD analysis, mostly for the more diluted sample with 3 wt% Ni. Increasing Ni content, as in the sample with 6 wt% Ni, the observed difference of the particle size estimated by the two

different methods is certainly related to the dipolar interactions between Ni nanoparticles (Fonseca et al. 2002, 2003). Such a feature is further supported by the temperature dependence of  $\chi(T)^{-1}$  shown in Fig. 4b. The most diluted sample ( $x = 3$  wt% Ni) exhibits a linear behavior, characteristic of paramagnetic materials that follows the Curie–Weiss law, for both ZFC and FC branches, which are essentially coincident for  $T > T_B$ . On the other hand, the sample with  $x = 6$  wt% Ni exhibits a much more pronounced separation of the ZFC and FC branches and the linear behavior is restricted to a narrower temperature range above  $T_B$ . In fact, it has been previously suggested that the concentration limit for a noninteracting system is  $\sim 4$  wt% (Masunaga et al. 2009).

Typical hysteresis loops  $M(H, T)$  for the sample Ni:SiO<sub>2</sub>–C with  $x = 3$  wt% Ni are displayed in Fig. 5. The data in the Fig. 5 clearly indicate that both the remanence and coercivity develop appreciably below  $T_B$  and that the coercivity field ( $H_C$ ) decreases with increasing temperature, being essentially zero for  $T > T_B$ . The experimental results suggest that  $M$  versus  $H$  curves are symmetric with respect to the applied magnetic field and possible exchange bias, due to an oxide NiO layer surrounding the Ni NP, has not been detected in our films. As far as this point is concerned, we mention that Ni NP with an oxide layer usually exhibit a magnetic

interaction between the ferromagnetic Ni and the antiferromagnetic NiO that is clearly observed as an asymmetry in  $M$  versus  $H$  curves (Cullity 1972). For the  $M$  versus  $H$  curve taken at  $T = 2$  K, the determined  $H_{C-}$  and  $H_{C+}$  were  $\sim -340$  and 343 Oe, respectively. Thus, considering the accuracy of the data it is possible to assume that  $|H_{C-}| \sim |H_{C+}|$  and that the Ni NP of the thin film with 3 wt% Ni is free from extra phases and of a NiO shell surrounding the Ni cores. It is important to mention that similar  $M$  versus  $H$  curves were obtained for the thin film with  $x = 6$  wt% Ni, further indicating that the polymeric precursor synthesis prevents the formation of an oxide layer in the Ni NP, a result similar to the one observed in powder Ni nanocomposites produced by the same method (Fonseca et al. 2002).

By computing the  $H_{C-}$  and  $H_{C+}$  values from several  $M$  versus  $H$  curves taken at several temperatures  $T < T_B$ , the temperature dependence of the coercivity field was constructed and the obtained diagram is displayed in Fig. 6. The behavior of  $H_C$  vs  $T^{1/2}$  indicates a thermally activated process with  $H_C$  increasing linearly for temperatures below  $\sim 6$  K, as inferred from the extrapolated value of  $T^{1/2}$  for  $H_C = 0$ . Such a temperature dependence of  $H_C$  is expected for systems comprised of randomly oriented and noninteracting nanoparticles and is given by (Gittleman et al. 1972):

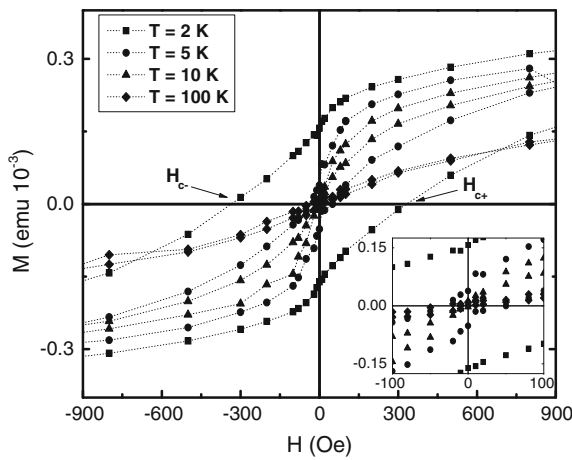


**Fig. 5** Hysteresis loops measured at 2, 5, 10, and 100 K for the Ni:SiO<sub>2</sub>–C thin film with  $x = 3$  wt% Ni. The inset shows an expanded view at low magnetic fields. The coercivity fields  $H_{C-}$  and  $H_{C+}$ , extracted from the negative and positive branches of the  $M$  versus  $H$  curves, respectively, are also indicated

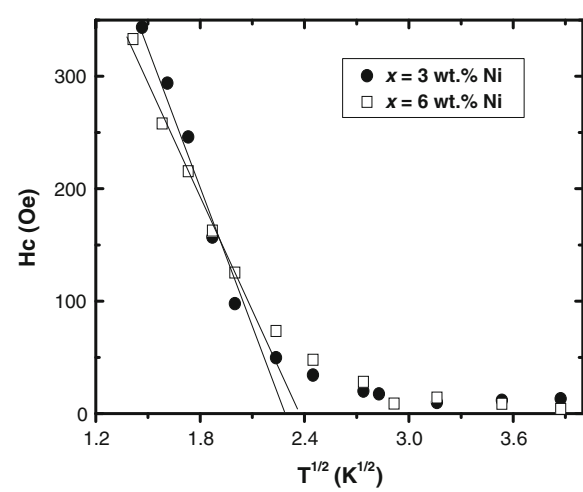


**Fig. 6** Temperature dependence of the coercivity field ( $H_C$ ) and best linear fits for the  $T < T_B$  temperature range for films Ni:SiO<sub>2</sub>–C with  $x = 3$  and 6 wt% Ni

$$H_C(T) = H_{C0} \left[ 1 - (T/T_B)^{1/2} \right] \quad (2)$$

with  $H_{C0} = 0.64 K_1^{\text{bulk}}/M_s$  (Bozorth 1956), where  $K_1^{\text{bulk}}$  is the anisotropy constant of bulk Ni described above,  $M_s$  is the saturation magnetization, and  $T_B$  given by Eq. 1.

Equation 2 also gives additional information regarding  $H_C$  at low temperatures. By using the appropriate expression  $H_{C0} = 0.64K_1/M_s$  and the Ni bulk value  $M_s(T=0) = 541 \text{ emu/cm}^3$ , we found  $H_{C0} \sim 950 \text{ Oe}$ . This zero-temperature coercivity field is similar to the ones obtained by the extrapolation of the  $H_C$  versus  $T^{1/2}$  curves (Fig. 5): 944 and 822 Oe for samples  $x = 3$  and 6 wt% Ni, respectively. The good agreement between the extrapolated  $H_{C0}$  values further indicates that the produced nanocomposite films exhibit features of a randomly oriented and noninteracting system of ferromagnetic particles, a characteristic more evident for the most diluted sample. The larger difference observed between the predicted and the lower experimental coercivities for the sample with  $x = 6$  wt% Ni extrapolated to  $T = 0$  may be related to weak magnetic interactions, which are expected to decrease  $H_{C0}$ .

## Conclusion

The experimental results of this study demonstrate that the polymeric precursor and spin coating techniques are suitable for the fabrication thin films of superparamagnetic nanocomposites comprised of fcc Ni particles embedded in a  $\text{SiO}_2$ –C matrix. Microstructural analyses revealed that that the films have homogenously distributed Ni particles with diameter  $<10 \text{ nm}$ . The nanometric size of Ni particles was confirmed by the superparamagnetic properties of the thin films, inferred from magnetization curves that clearly exhibit blocking temperatures  $\sim 10 \text{ K}$ . As inferred from both microstructural analyses and magnetic measurement, Ni nanoparticles are believed to be free from an oxide layer, a desirable feature for practical applications. A model of randomly oriented and noninteracting ferromagnetic particles was found to describe the temperature dependence of the coercivity, indicating that magnetic interactions in the films with low Ni content (3 wt%) are essentially absent.

**Acknowledgments** This work was supported by the Brazilian agencies FAPESP/CEPID, CNPq/PRONEX, and CAPES. RFJ, FCF, MTE, ERL, and EL are Conselho Nacional de Desenvolvimento Científico e Tecnológico (CNPq) fellows.

## References

- Almeida RM, Marques AC, Ferrari M (2003) Optical nano-composite planar waveguides doped with rare-earth and noble metal elements. *J Sol-Gel Sci Technol* 26:891–896
- Bozorth RM (1956) Ferromagnetism, Chap. 18. Van Nostrand, Princeton, p 831
- Carreño NLV, Leite ER, Santos LPS, Lisboa-Filho PN, Longo E, Araújo GCL, Barison A, Ferreira AG, Valentini A, Probst LFD (2002) Synthesis, characterization and study of magnetic and catalytic properties of dispersed Ni nanoparticles on mesoporous  $\text{SiO}_2$  matrix. *Quim Nova* 25:935–942
- Cullity JBD (1972) Introduction to magnetic materials. Addison-Wesley, Reading
- Dureuil V, Ricolleau C, Gandais M, Grigis C, Lacharme JP, Naudon A (2001) Growth and morphology of cobalt nanoparticles on alumina. *J Cryst Growth* 233:737–784
- Fonseca FC, Goya GF, Jardim RF, Muccillo R, Carreño NLV, Longo E, Leite ER (2002) Superparamagnetism and magnetic properties of Ni nanoparticles embedded in  $\text{SiO}_2$ . *Phys Rev B* 66:104406
- Fonseca FC, Goya GF, Jardim RF, Carreño NLV, Longo E, Leite ER, Muccillo R (2003) Magnetic properties of Ni: $\text{SiO}_2$  nanocomposites synthesized by a modified sol-gel method. *Appl Phys A* 76:621–623
- Fonseca FC, Ferlauto AS, Alvarez F, Goya GF, Jardim RF (2005) Morphological and magnetic properties of carbon-nickel nanocomposite thin films. *J Appl Phys* 97:044313
- Gittleman JI, Goldstein Y, Bozowski S (1972) Magnetic properties of granular nickel films. *Phys Rev B* 5: 3609–3621
- Gouveia PS, Escote MT, Longo E, Leite ER, Carreño NLV, Fonseca FC, Jardim RF (2005) Síntese e Caracterização de Nanocompósitos Ni: $\text{SiO}_2$  processados na Forma de Filmes Finos. *Quim Nova* 28:842–846
- Hong S, Mirkin CA (2000) A nanoplotter with both parallel and serial writing capabilities. *Science* 288:1808–1811
- Kockrick E, Krawiec P, Schnelle W, Geiger D, Schappacher FM, Pöttgen R, Kaskel S (2007) Space-confined formation of FePt nanoparticles in ordered mesoporous silica SBA-15. *Adv Mater* 19:3021–3026
- Lee JS, Kim BS (2001) Synthesis and related kinetics of nanocrystalline Ni by hydrogen reduction of NiO. *Mater Trans JIM* 42:1607–1612
- Liu X, Fu L, Hong S, Dravid VP, Mirkin CA (2004) Arrays of Magnetic Nanoparticles via ‘Dip-Pen’ Nanolithography. *Adv Mater* 14:231–234
- Masunaga SH, Jardim RF, Fichtner PFP, Rivas J (2009) Role of dipolar interactions in a system of Ni nanoparticles studied by magnetic susceptibility measurements. *Phys Rev B* 80:184428
- Munford ML, Seligman L, Sartorelli ML, Voltolini E, Martins LFO, Schwarzacher W, Pasa AA (2001) Electrodeposition

- of magnetic thin films of cobalt on silicon. *J Magn Magn Mater* 226–230:1613–1615
- Osaka T (2000) Electrodeposition of highly functional thin films for magnetic recording devices of the next century. *Electrochim Acta* 45:3311–3321
- Rangel JH, Carreño NLV, Leite ER, Longo E, Campos CEM, Lanciotti F Jr, Pizani PS, Varela JA (2002) Photoluminescence in amorphous (PbLa)TiO<sub>3</sub> thin films deposited on different substrates. *J Lumin* 99:7–12
- Sharma SK, Vargas JM, Knobel M, Pirotta KR, Meneses CT, Kumar S, Lee CG, Pagliuso PG, Rettori C (2010) Synthesis and tuning the exchange bias in Ni–NiO nanoparticulate systems. *J Appl Phys* 107:09D725
- Skumryev V, Stoyanov S, Zhang Y, Hadjipanayis G, Givord D, Nogués J (2003) Beating the superparamagnetic limit with exchange bias. *Nature* 243:850–853
- Stoner EC, Wohlfarth EP (1948) A mechanism of magnetic hysteresis in heterogeneous alloys. *Philos Trans R Soc Lond Ser A* 240:599–642
- Tomita S, Hagiwara M, Kashiwagi T, Tsuruta C, Matsui Y, Fujii M, Hayashi S (2004) Ferromagnetic resonance study of diluted Fe nanogranular films. *J Appl Phys* 95:8194–8198
- Zanetti SM, Leite ER, Longo E, Varela JA (1999) Origin of cracks developed during SrTiO<sub>3</sub> thin film preparation from polymeric precursors. *Appl Organomet Chem* 13:373–382
- Zhu PL, Xue F, Liu Z, Fan YL, Jiang ZM, Yang XJ (2009) Influence of annealing atmosphere on the magnetic properties of SiO<sub>2</sub>/Fe/SiO<sub>2</sub> sandwiched nanocomposite films. *J Appl Phys* 106:043907